PCCP

ROYAL SOCIETY OF CHEMISTRY

PAPER

View Article Online
View Journal | View Issue

Cite this: *Phys. Chem. Chem. Phys.*, 2024, **26**, 2915

The plasmonic effect of Cu on tuning CO_2 reduction activity and selectivity†

Jing Xue,[ab] Zhenlin Chen,[ab] Kun Dang,[ab] Lei Wu,[ab] Hongwei Ji,[ab] Chuncheng Chen,[ab] Yuchao Zhang *[ab] and Jincai Zhao[ab]

Received 10th November 2023,
Accepted 19th December 2023

DOI: 10.1039/d3cp05450k

rsc.li/pccp

Copper (Cu) has been widely used for catalyzing the CO_2 reduction reaction (CO_2RR), but the plasmonic effect of Cu has rarely been explored for tuning the activity and selectivity of the CO_2RR. Herein, we conducted a quantitative analysis on the plasmon-generated photopotential (E_{hv}) of a Cu nanowire array (NA) photocathode and found that E_{hv} exclusively reduced the apparent activation energy (E_a) of reducing CO_2 to CO without affecting the competitive hydrogen evolution reaction (HER). As a result, the CO production rate was enhanced by 52.6% under plasmon excitation when compared with that under dark conditions. On further incorporation with a polycrystalline Si photovoltaic device, the Cu NA photocathode exhibits good stability in terms of photocurrent and syngas production ($CO:H_2 = 2:1$) within 10 h. This work validates the crucial role of the plasmonic effect of Cu on modulating the activity and selectivity of the CO_2RR.

1. Introduction

Plasmonic catalysis has emerged as a promising field where solar energy is efficiently harnessed to drive chemical reactions.[1,2] Specifically, the localized surface plasmon resonance (LSPR) phenomenon occurs when a beam of light interacts with metal nanostructures smaller than the wavelength of the incident light, inducing collective oscillation of free electrons on metal surfaces.[3,4] After light irradiation, plasmons decay through non-radiation pathways, enhancing surface electromagnetic field, forming hot carriers (electron–hole pairs), and inducing photothermal effects.[5–8] Plasmonic metals, such as noble metal gold (Au) and silver (Ag), are recognized as efficient mediators for utilizing solar energy due to their exceptional capability in harvesting a broad spectrum ranging from the ultraviolet-visible (UV-vis) to near-infrared (NIR) region, and are thereby widely researched in water splitting,[9–12] ethylene epoxidation,[13,14] NH_3 decomposition,[15] and so on.[16–19] However, the scarcity of Au and Ag metals hinders their practical applications. Non-noble metals, particularly copper (Cu), that also exhibit an excellent LSPR effect from the UV-vis to NIR region, present promising opportunities for replacing noble metals in plasmonic catalysis.[20,21]

The concept of carbon neutrality has been proposed to mitigate the escalating atmospheric CO_2 levels and convert it into value-added products, thereby achieving the goals of environmental protection and energy storage.[22,23] The plasmon-assisted CO_2 reduction reaction (CO_2RR) provide a sustainable and environmentally friendly approach by harnessing solar energy.[24,25] Plasmon-assisted CO_2RR systems, such as Au@Ru core–shell nanoflowers and Ag nanopyramids,[26–28] have shown great potential not only in improving the activity but also in enhancing the selectivity, as described in several reports. The increase in activity (including current density and product yield) is commonly attributed to the presence of hot carriers or photothermal effects. The selective transfer of hot carriers into antibonding orbitals of the specific surface adsorbates may regulate the reaction path and accelerate chemical reactions by weakening certain chemical bonds.[29,30] Plasmon-induced local heating excites the vibrational transitions of all the reactants and accelerates the overall chemical reactions.[31,32] It is important to distinguish between hot carrier effects and photothermal effects, as it is crucial for design guidelines for the further optimization of plasmonic nanomaterials.[29,33] By analyzing the behavior of the plasmon-induced photocurrent, Tian's group ascribed the rapid response (in the time scale of milliseconds) of photocurrent to the hot carrier effect and the slow response of photocurrent (in the time scale of seconds) to the photothermal effect.[32] The utilization of the plasmon-assisted CO_2RR can further modulate the product selectivity, facilitating the formation of single/multi-carbon products while suppressing the hydrogen evolution reaction (HER). Cu has been widely studied as an electrocatalyst in the CO_2RR,[34–36] while there is little research on the plasmonic effect of Cu on the CO_2RR. The quantitative

[a] *Key Laboratory of Photochemistry, Beijing National Laboratory for Molecular Sciences, Institute of Chemistry, Chinese Academy of Sciences, Beijing 100190, P. R. China. E-mail: yczhang@iccas.ac.cn*
[b] *University of Chinese Academy of Sciences, Beijing 100049, P. R. China*

† Electronic supplementary information (ESI) available: Additional experimental details, chemicals, formula derivation, PEC experiments of Cu NAs by CA and *i–t* measurements. See DOI: https://doi.org/10.1039/d3cp05450k

analysis of the contribution of light and unraveling the mechanism of selectivity changes induced by plasmon excitation remain elusive.

The Cu nanowire array (NA) electrode synthesized *in situ* is anisotropic, displaying two LSPR absorption peaks corresponding to plasmonic resonance in the longitudinal and transverse directions. Besides, many previous studies show that light absorption can be tuned by varying the nanowire diameter and the angle of light incidence.[21,37] These advantages of the Cu NAs allow for more flexibility in the optimization of its photoelectrochemical (PEC) activity, endowing it with great potential to be an ideal plasmonic catalyst for the CO_2RR. In this work, Cu NAs were employed as a plasmonic catalyst for the CO_2RR, where Cu NAs simultaneously acted as electrocatalysts and light absorbers. We observed that visible light excitation of the Cu NA photocathode enhanced the activity and selectivity of the CO_2RR and inhibited the competitive HER. By combining PEC techniques, including current differential curve, step potential, and electrochemical impedance experiments, we resolved the contribution of hot carrier effects from photothermal effects. The accumulation of hot electrons resulted in the generation of cathodic photopotential (E_{hv}), about 34.6 mV at -0.8 V_{RHE} under 3.0 W cm^{-2} of visible light. The E_{hv} caused lower energy barriers for CO generation (reduced from 26.61 to 18.95 kJ mol^{-1}). Furthermore, when combined with a Si-based solar cell and an Au/TiO_2 photoanode, the Cu NA photocathode exhibited a stable photocurrent density of 8.8 mA cm^{-2} and generated syngas with a CO/H_2 molar ratio of 2 : 1 within 10 h. These findings provide insights into the mechanistic role of plasmon excitation of Cu in catalyzing the CO_2RR.

2. Materials and methods

2.1. Preparation of Cu nanowire array catalysts

The Cu NAs were prepared by a template-assisted electrodeposition method. The Cu foil was covered with an anodic aluminum oxide (AAO) template, then another Cu foil was added on the AAO template to form a sandwich-like structure. The electrodeposition process was carried out in a two-electrode system. One Cu foil substrate was covered with an AAO template as a counter electrode and another Cu foil as a working electrode. Cu was filled into the channels of the AAO template by applying a constant voltage of 0.35 V for 1200 s in 0.5 M $CuSO_4{\cdot}5H_2O$ and 0.1 M H_3BO_3 electrolyte. After deposition, the sample was placed in 1 M NaOH for 2 h to dissolve the AAO template. The sample was rinsed in deionized water and dried using Ar. As a result, vertically aligned Cu NAs were obtained on the Cu foil. Finally, Cu NAs were further annealed at 473 K in an air atmosphere for 2 h to obtain a stable photocathode.

2.2. PEC reduction process

The CO_2RR experiment was performed in a custom-made gas-tight H-type cell, which was composed of two compartments that were separated by a proton exchange membrane (Nafion-117). Each H-cell chamber was equipped with 20 mL of 0.1 M $KHCO_3$. The reference electrode was Ag/AgCl (3 M KCl), and the counter electrode was a graphite rod electrode. The geometric area of the working electrode (Cu NAs) exposed to electrolytes was controlled at 0.5 cm^2. Before the CO_2RR measurements, CO_2 gas was continuously purged into two compartments for at least 30 min to reach saturation (pH = 6.8). The stirring magnet rotated at a speed of 2000 rpm in the cathode chamber during the CO_2RR measurement, and a mass flow controller was used to maintain a constant flow rate of 10 sccm for CO_2. All PEC measurements were carried out at an electrochemical workstation (CHI 760E). The electrode potential was converted into the potential of reversible hydrogen electrode (RHE) following the conversion relationship: $E_{RHE} = E_{Ag/AgCl} + 0.059 \times pH + 0.197\ V - iR$ drop (R is the solution resistance of 0.1 M $KHCO_3$, which was obtained by electrochemical impedance spectroscopy (EIS) measurement). Linear sweep voltammetry (LSV) curves were obtained at a scan rate of 20 mV s^{-1} to qualitatively evaluate the catalytic activity under both dark and light conditions. The potential-step experiment was carried out by multi-potential steps using an appropriate step potential (5 mV) for the various potentials with a pulse width of the step potential of 5 s. The frequency range of EIS was from 5000 to 0.1 Hz with an amplitude of 5 mV at different potentials. The double layer capacitance (C_{dl}) was obtained by the cyclic voltammetry (CV) method. The potential window of the CV curves ranged from 0.15 to 0.25 V_{RHE}, with scan rates varying from 5 to 30 mV s^{-1}. The effect of light irradiation on the photocurrent was investigated at a regular interval of 20 s for light on/off. A 300 W Xenon lamp (Beijing China Education AU-LIGHT Technology Co., Ltd) with an AM 1.5G filter was used as the light source. All Cu NA electrodes were pre-electrochemically reduced at -1.0 V_{RHE} until the current stabilized before conducting PEC measurements.

2.3. Solar-driven PEC device for the CO_2RR

The CO_2RR was carried out in a typical H-type solar cell, in which the Cu NA electrode was placed in the cathode cell filled with 0.1 M $KHCO_3$, while an Au/TiO_2 photoanode was placed in a 0.5 M potassium borate buffer electrolyte. The light source was simulated sunlight with a 300 W Xenon lamp coupled with an AM 1.5G filter. A 53 $\times$ 30 mm polycrystalline Si solar cell, with a maximum open circuit voltage of 3 V, was exposed to visible light irradiation to generate the required voltage.

2.4. CO_2RR product analysis

The exhaust trachea was connected to the gas chromatography instrument (GC, Fuli GC9790 Plus) for quantitative analysis of gas products. CO, C_2H_4 and C_2H_6 were detected using a flame ionization detector (FID) and H_2 was detected using a thermal conductivity detector (TCD). The liquid product (HCOOH) was analyzed quantitatively by ion chromatography (IC). The faradaic efficiency (FE) of the gas product was calculated as follows:

$$\mathrm{FE}\ (\%) = \frac{\text{quantity of the product} \times n \times F}{Q} \times 100\%$$

where n is the number of electrons transferred, F is the Faraday constant (96 485 C mol^{-1}), and Q represents the total coulomb of electrons passing through the working electrode.

3. Results and discussion

3.1. Morphology and structure analyses

As shown in Fig. 1a, Cu NAs were synthesized by a template-assisted electrodeposition method.[38] Scanning electron microscopy (SEM) images in Fig. 1b and c show that the diameter of Cu NA is about 70 nm and the length is 10 μm. Furthermore, high-resolution transmission electron microscopy (HRTEM) revealed that Cu NAs had a lattice fringe with an interplane spacing of 0.18 nm, corresponding to the (200) facet of metallic Cu (Fig. 1d). The UV-vis diffuse reflectance spectrum was tested as the evidence of the absorbance characteristics of plasmonic metals. As shown in Fig. 1e, Cu NAs exhibited wide absorption in the wavelength range of 350–800 nm. The small absorption peak from 500 to 570 nm with maximum absorption at 540 nm was ascribed to the transverse resonance absorption of Cu NAs. As Duan *et al.* proved,[37] plasmonic Cu NAs exhibit two LSPR absorption peaks corresponding to plasmonic resonance in the longitudinal and transverse directions. When the wave vector of the incident light is parallel to the Cu NAs, only transverse modes can be excited. After the PEC reduction process, the LSPR absorption peak position of Cu NAs did not shift. However, the absorption intensity slightly decreased, which is related to the change of the electrode surface color from black (Cu^{2+}) to reddish brown ($Cu^{0/1+}$). The Cu NAs were also monitored with X-ray diffraction (XRD) and X-ray photoelectron spectroscopy (XPS) techniques to study the crystal structure and valence states of the obtained samples (Fig. 1f and g). The synthesized Cu NAs had a polycrystalline structure with Cu^{+} and Cu^{2+} presented on the surfaces. After the PEC reduction process, the Cu NAs were predominantly composed of the (200) facet and showed metallic valence state. Meanwhile, rough surfaces were formed due to the deoxidation of $Cu^{1+/2+}$ during the PEC reduction process (Fig. S1, ESI†). This phenomenon of surface unevenness is consistent with the findings reported by Huang *et al.*[39] The uneven surface can provide more active sites, which is beneficial for the CO_2RR performance.[40]

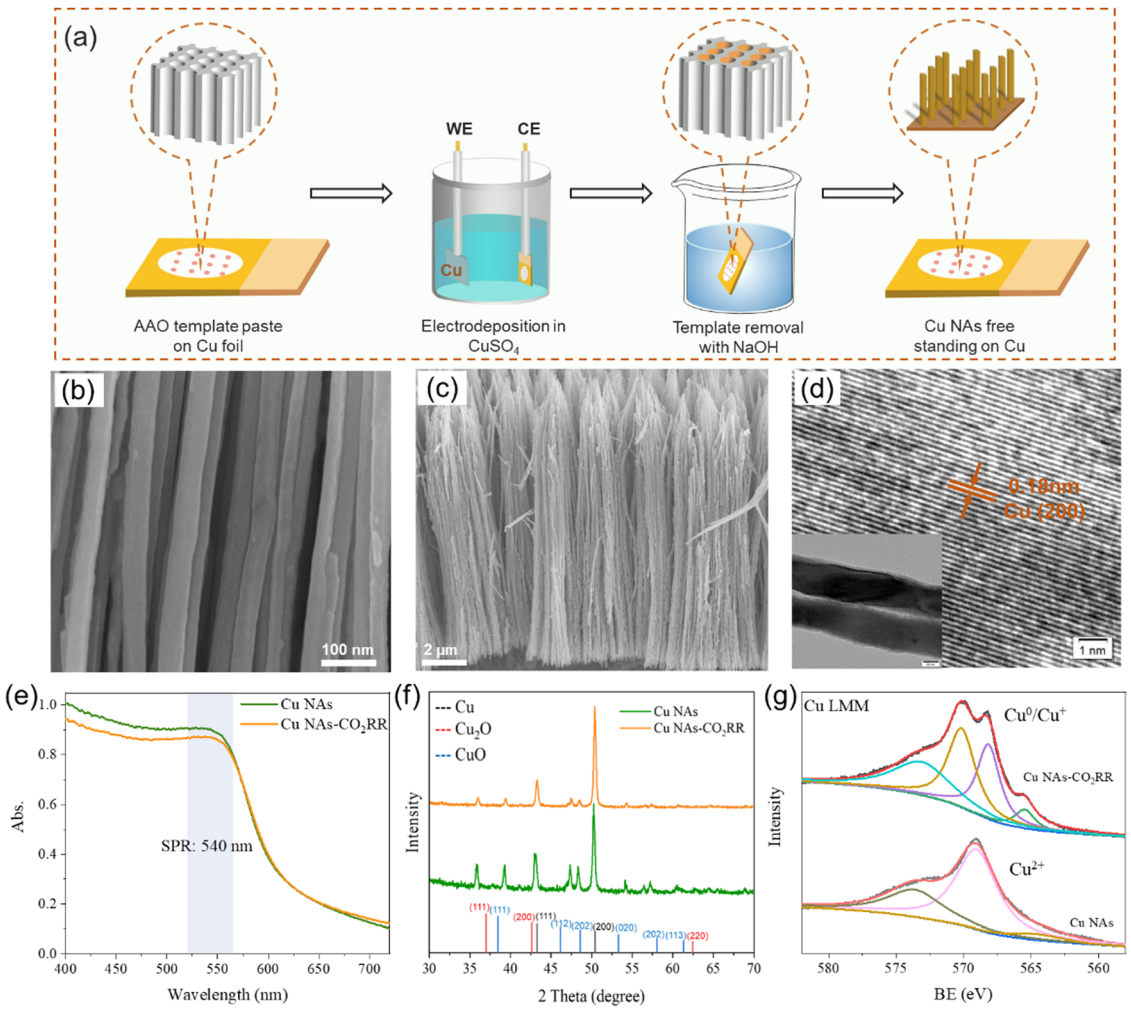

Fig. 1 (a) Schematic diagram of Cu NAs synthesized by the template-assisted electrodeposition method, with anodic aluminum oxide (AAO) as the template. (b) and (c) SEM images and (d) HRTEM images of Cu NAs. (e) UV-Vis diffuse reflectance spectra and (f) XRD patterns of Cu NAs before (green) and after the PEC reduction process (orange). (g) Cu LMM patterns of Cu NAs before (bottom) and after the PEC reduction process (top).

3.2. PEC tests for quantitative analysis of plasmonic effects

The photo-response induced by the LSPR effect was first compared between the Cu NA photocathode and a commercial Cu foil using linear sweep voltammogram (LSV) measurements in a CO_2-saturated 0.1 M $KHCO_3$ electrolyte (Fig. 2a). The Cu NAs exhibited a remarkable photo-response, showing an increase in current density upon LSPR excitation (3.0 W cm^{-2}) compared to the dark conditions, while the current density of the Cu foil remained relatively unchanged under light irradiation. These results were consistent with the measured chronoamperometry (CA) curves under chopped light irradiation at -0.7 V_{RHE} (Fig. 2b), in which $\Delta j_{Cu\ NAs}$ = 0.7 mA cm^{-2}, and $\Delta j_{Cu\ foil}$ = 0 mA cm^{-2} ($\Delta j = j_{photo} - j_{dark}$). Tafel analysis showed that the Cu NA photocathode exhibited a slope of 190.1 mV dec^{-1} in the dark (Fig. 2c). Upon LSPR excitation, the Tafel slope decreased by about 10.9 mV dec^{-1}, indicating that light excitation promotes a faster reaction kinetics.[41] In contrast, the Tafel slope of the Cu foil remained unchanged under light irradiation, confirming the lack of photo-response on the Cu foil.

The contribution of the hot carrier effect and the photothermal effect was investigated. As shown in Fig. 2d, the photocurrent of the Cu NA photocathode responded immediately upon LSPR excitation, reaching its maximum value within 5 ms, and the current differential curve showed a sharp change. However, the photothermal-induced photocurrent responded much slower (seconds) due to the slow thermal diffusion in surroundings.[29,32] Therefore, the measured photocurrent is mainly the contribution of hot carriers. To further eliminate the contribution of photothermal effects, we conducted CA measurements at various temperatures under chopped light irradiation (Fig. S2, ESI†). The control experiment showed that an increase in temperature led to a corresponding current increase in the dark. However, it was worth noting that when the temperature increased from 298 to 313 K, Δj remained around 0.53 mA cm^{-2} at -0.6 V_{RHE}. This observation suggests that there is no direct correlation between the increase in temperature and the enhancement of Δj, implying a minimal contribution of the photothermal effect to the generation of photocurrent.

The value of j_{photo} is determined by the applied light intensity (I), and a simple quantitative model has been reported as shown in the Formula derivation section of the ESI† (eqn (S1)–(S5)). We obtained CA curves for the Cu NA photocathode with different light intensities at -0.7 V_{RHE} under chopped light irradiation (Fig. S3, ESI†), and drew a curve of j_{photo} as a function of light intensity (Fig. 3a). The results showed super-linear relationship between light intensity and j_{photo}, which served as a distinctive feature of the hot-carrier-driven redox reaction of plasmonic nanomaterials. Accordingly, the photochemical conversion coefficient Φ (s cm^2 mol^{-1}) was determined by plotting $RT\ln(j_{photo})$ against light intensity.[16,42] The slope of the plot gave a Φ of approximately 258.7 s cm^2 mol^{-1}, indicating that LSPR excitation of an incident intensity of 1.0 W cm^{-2} contributed about 0.26 kJ mol^{-1} to the free energy of the reaction (Fig. S4, ESI†).

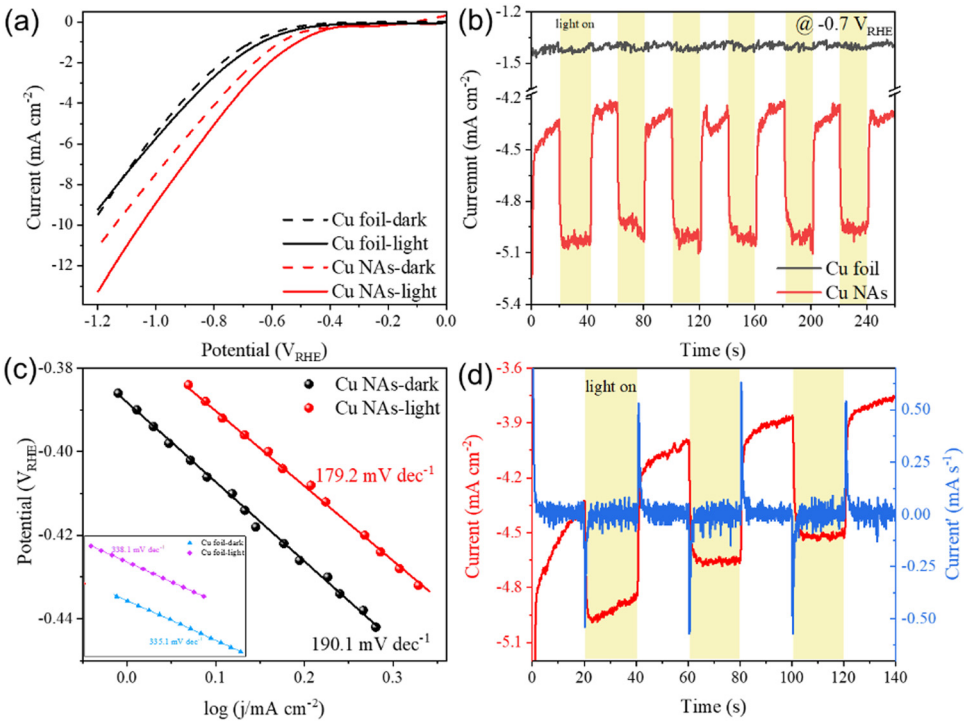

Fig. 2 (a) LSV curves of the Cu foil (black) and Cu NA (red) photocathodes from 0.0 to -1.2 V_{RHE} with (solid lines) and without (dashed lines) light irradiation in CO_2-saturated 0.1 M $KHCO_3$. (b) CA measurements of the Cu foil (black) and Cu NA (red) photocathodes at -0.7 V_{RHE} under chopped light irradiation. (c) Tafel plots for the Cu NA and Cu foil photocathodes (inset) with and without light irradiation. (d) The CA measurement of the Cu NA photocathode under chopped light irradiation (red) and its differential (blue) at -0.7 V_{RHE}.

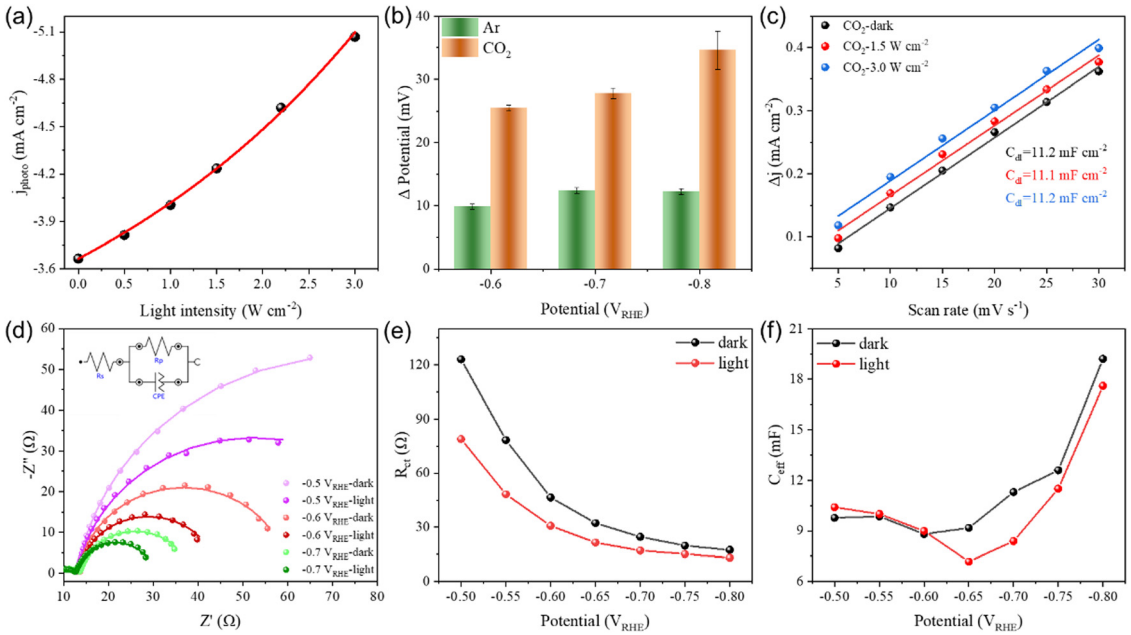

Fig. 3 (a) The photocurrent density plotted as a function of the incident light intensity. (b) Step potential required to achieve consistent changes in plasmon-assisted photocurrent with Ar and CO_2 atmosphere at different applied potentials. (c) Double layer capacitance of Cu NAs with and without light irradiation. (d) Nyquist plots of EIS measurements (points) and fitted (lines) with the equivalent circuit (inset) curve for Cu NAs at different applied potentials in the dark (light colors) and under light irradiation (deep colors). Fitted parameters of R_{ct} (e) and C_{eff} (f) from the Nyquist plots.

Plasmonic Cu generates hot electrons and holes under light excitation. Hot holes are transferred to the counter electrode through an external circuit assisted by the applied bias, while hot electrons accumulate on the surface of Cu NAs. After that, a stable electron distribution with Fermi levels higher than those under the dark conditions was obtained, generating a cathode photopotential (E_{hv}).[32] The potential step method enables the simulation of photocurrent behaviour and determination of the value of E_{hv}, in which changes in current (ΔI) was obtained by adjusting the step potential (ΔP) in the dark (Fig. S5a, ESI†). Accordingly, E_{hv} could be calculated based on the observed changes of photocurrent under light conditions. The linear relationship between ΔI and ΔP in the dark is shown in Fig. S5b (ESI†), and the increase in current caused by illumination is shown in Fig. S5c (ESI†). As summarized in Fig. 3b, the E_{hv} increased from 25.5 mV at -0.6 V_{RHE} to 34.6 mV at -0.8 V_{RHE}, indicating that the applied potential caused the increase of E_{hv}. Furthermore, a large difference was observed between the values of E_{hv} under Ar (12.2 mV) and CO_2 (34.6 mV) atmospheres at -0.8 V_{RHE}, suggesting that the presence of a CO_2 atmosphere plays a crucial role in enhancing the separation of hot carriers.

To further illustrate the effect of CO_2 atmosphere on the separation of hot carriers, transient photovoltage (TPV) and transient photocurrent experiments were conducted in Ar and CO_2 atmospheres (Fig. S6, ESI†).[43] The fitted time attenuation constant was enhanced to 362.7 ns compared to that for the CO_2-free condition (312.2 ns), and the calculated value of Δj was greater in CO_2 atmosphere (Δj_{CO_2} = 0.83 mA cm^{-2}) than in Ar atmosphere (Δj_{Ar} = 0.53 mA cm^{-2}) at -0.7 V_{RHE}. These results confirmed that the CO_2 atmosphere promoted hot carrier separation.

The generation of E_{hv} is reported to supply electrons either for the charging of the electrode/electrolyte double layer or driving faradaic reactions.[9] To determine whether the hot electrons were involved in the charging process of the double layer, we tested the CV curves of the non-faradaic region at different scan rates with and without light irradiation (Fig. S7, ESI†). The double layer capacitance (C_{dl}) was obtained from the slope of current density corresponding to different scan rates.[44] The C_{dl} values of Cu NAs under both dark and light conditions were both 11.2 mF cm^{-2}, as shown in Fig. 3c. The result suggested that the E_{hv} generated by light irradiation did not contribute to the C_{dl} component, but was solely utilized for faradaic reactions.

The interfacial hot-electron transfer kinetics was analyzed by using EIS,[9] and the Nyquist plots were obtained in the dark and under light conditions at various potentials. The arc radius of the Nyquist plot in the presence of light was smaller than that under the dark conditions (Fig. 3d), suggesting that the charge-transfer process was facilitated by the participation of hot electrons. Further equivalent circuit fitting also proved that the charge-transfer resistance (R_{ct}) could be reduced under light irradiation (Fig. 3e and Table S1, ESI†). The capacitance value is another critical parameter that closely correlates with variations in the amount of surface adsorbed species (such as *CO, Fig. S8, ESI†).[45,46] It is reported that the effective capacitance (C_{eff}) value is related to "surface cleanliness", in other words, an increase in the number of adsorbed species on the surface will lead to a decrease in

the C_{eff} value.[26] Due to the larger aspect ratio of Cu NAs, the electrochemical active surface area is significantly enlarged, resulting in a higher C_{eff} (on the order of mF) compared to spherical nanomaterials reported in the literature (on the order of μF).[47] The C_{eff} values increased significantly with the increase of potentials after −0.65 V_{RHE} under both dark and light conditions, as depicted in Fig. 3f, indicating a surface with reduced adsorbed species. More importantly, C_{eff} decreased from 11.3 to 8.4 mF at −0.7 V_{RHE} under light irradiation, indicating an increase in the amount of surface adsorption species of *CO.

3.3. Plasmon-assisted CO_2RR performance

The CO_2 reduction products on the Cu NA photocathode were analyzed by using online gas chromatography (GC) and ion chromatography (IC) at various potentials ranging from −0.6 to −1.4 V_{RHE} (Fig. S9–S11, ESI†). Carbon monoxide (CO) and formate ($HCOO^-$) were the main reduction products, with a small amount of C_2 (C_2H_4, C_2H_6) yield. It is worth noting that light excitation of the plasmonic Cu NAs with 420 nm ≤ λ ≤ 800 nm (3.0 W cm^{-2}) induced a marked change in the FE of products (especially for H_2 and CO) compared to that observed during dark electrocatalysis (Fig. S12 and Table S2, ESI†). Specifically, we observed a decrease in the FE for H_2 evolution concomitantly with an increase in the FE for CO at all applied potentials. The lowest FE of H_2 was observed at −0.8 V_{RHE}, and the FE of H_2 decreased from 24.2% in the dark to 20.6% under light irradiation (Fig. 4a). The decrease in HER activity was accompanied by an enhancement in the selectivity for CO_2RR. The FE of CO increased by 11.4% compared to that observed

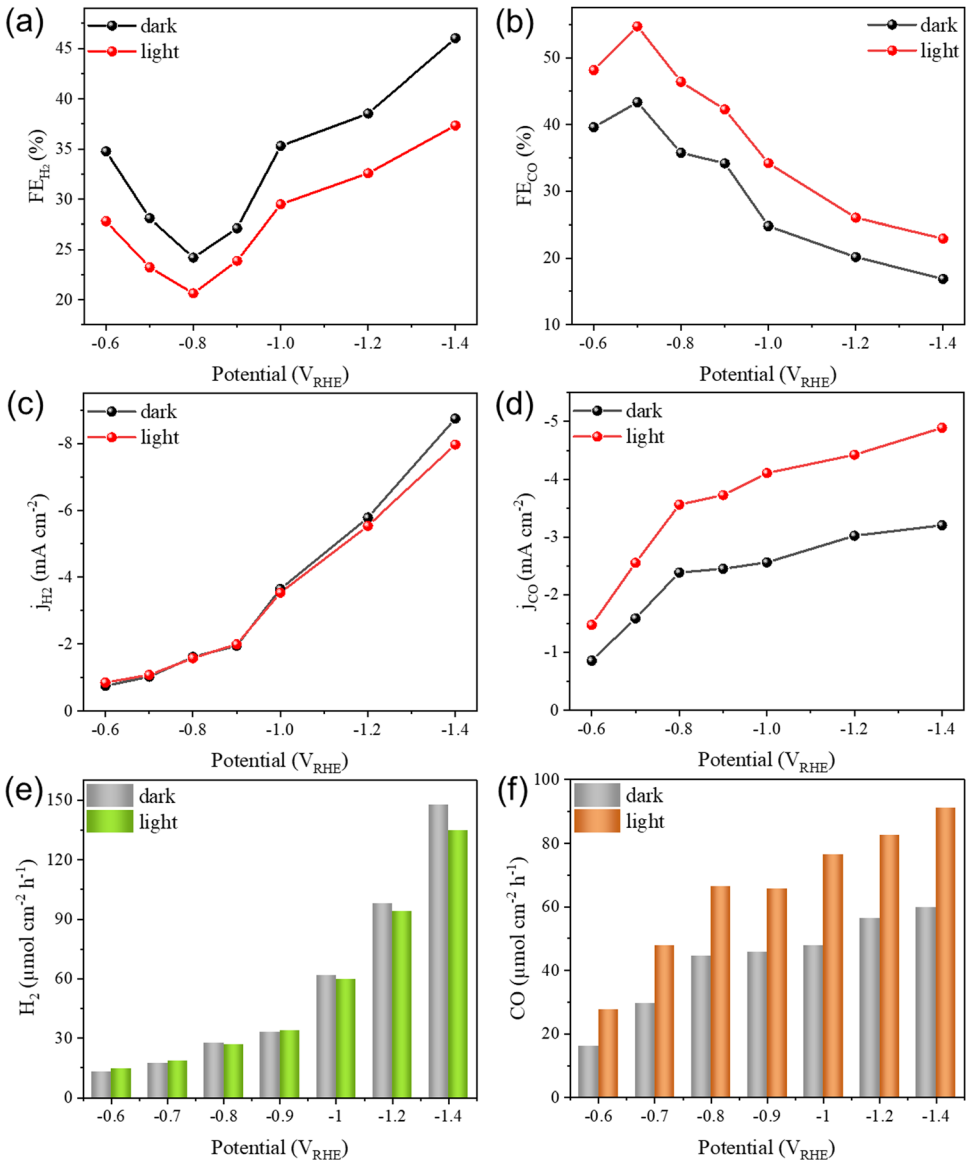

Fig. 4 The FE (a) and (b), partial current density (c) and (d), and production rate (e) and (f) of H_2 and CO in the dark and under light irradiation at different applied potentials.

without light and accounted for 54.7% of the total products (Fig. 4b). The partial current densities associated with H_2 (j_{H_2}) and CO (j_{CO}) are shown in Fig. 4c and d. We only observed very little change in j_{H_2} between dark and light conditions, but there was a noticeable increase in j_{CO}. At −1.4 V_{RHE}, the j_{CO} was increased by 53.1%, from 3.2 mA cm^{-2} in the dark to 4.9 mA cm^{-2} under light irradiation. Correspondingly, the production rate of CO was increased by 52.6%, from 59.8 μmol cm^{-2} h^{-1} in the dark to 91.2 μmol cm^{-2} h^{-1} under light irradiation (Fig. 4e), while the production rate of H_2 did not change significantly (Fig. 4f and Fig. S13, ESI†). These findings demonstrated that the light irradiation of the Cu NA photocathode preferentially enhanced the catalytic activity towards the CO_2RR without affecting the HER across all applied potentials. The CO_2 reduction products on the Cu foil were analyzed under different applied potentials in the dark and under light irradiation. The FE of all products (including H_2, CO, HCOOH, CH_4, and C_2) under light irradiation was almost unchanged compared with that dark conditions (Fig. S14, ESI†), which also proved that Cu foil has no photo-response.

Syngas composed of CO/H_2 with different molar ratios can be precisely tailored to match downstream chemical processes to get value-added chemicals.[48–50] For example, a molar ratio of $CO:H_2 = 1:2$ can be used to synthesize olefins and alcohols, while a molar ratio of $CO:H_2 = 2:1$ can produce short-chain hydrocarbon. The CO/H_2 molar ratio in our study could be adjusted from 0.40 to 1.70 in the dark and from 0.67 to 2.60 under light irradiation (Fig. S15, ESI†). Therefore, the strategy of plasmon excitation offers a novel approach for both promoting CO_2RR and regulating product composition.

3.4. Effect of plasmon excitation on the reaction mechanism

To gain insights into the energetics involved in the plasmon-assisted hot electron transfer reaction, we measured the apparent activation energy (E_a) for the reaction in the dark and under light irradiation. The reaction rate was measured as a function of temperature ranging from 288 to 313 K with an interval of 5 K (Fig. S16, ESI†). The slope obtained by linear fitting of each Arrhenius plot was used to determine E_a.[42,51] It was noted that the E_a was reduced from 26.61 to 18.95 kJ mol^{-1} upon LSPR excitation for the generation of CO (Fig. 5a), confirming that the LSPR excitation on the Cu NA photocathode efficiently reduces the energy barrier for CO_2RR. However, as shown in Fig. 5b, the change of E_a for the HER was minimal (varies from 26.42 to 25.66 kJ mol^{-1} under light irradiation).

To better illustrate the mechanism of the plasmon-assisted CO_2RR, reaction free energy profiles are depicted in Fig. 5c. CO is the main CO_2RR product *via* a two-electron pathway, and the process of reducing CO_2 to CO goes along CO_2 → *CO_2 → *COOH → *CO → CO.[43,52] First, the adsorption of CO_2 on the surface of the Cu NA photocathode begins with an electron transfer, forming *$CO_2^{\delta-}$, which is also considered as the rate determining step (RDS). The transfer of a proton leads to the formation of *COOH, followed by a second proton-coupled electron transfer that results in the formation of *CO. Finally, *CO desorbs to form CO gas. As obtained from Fig. 5a, the

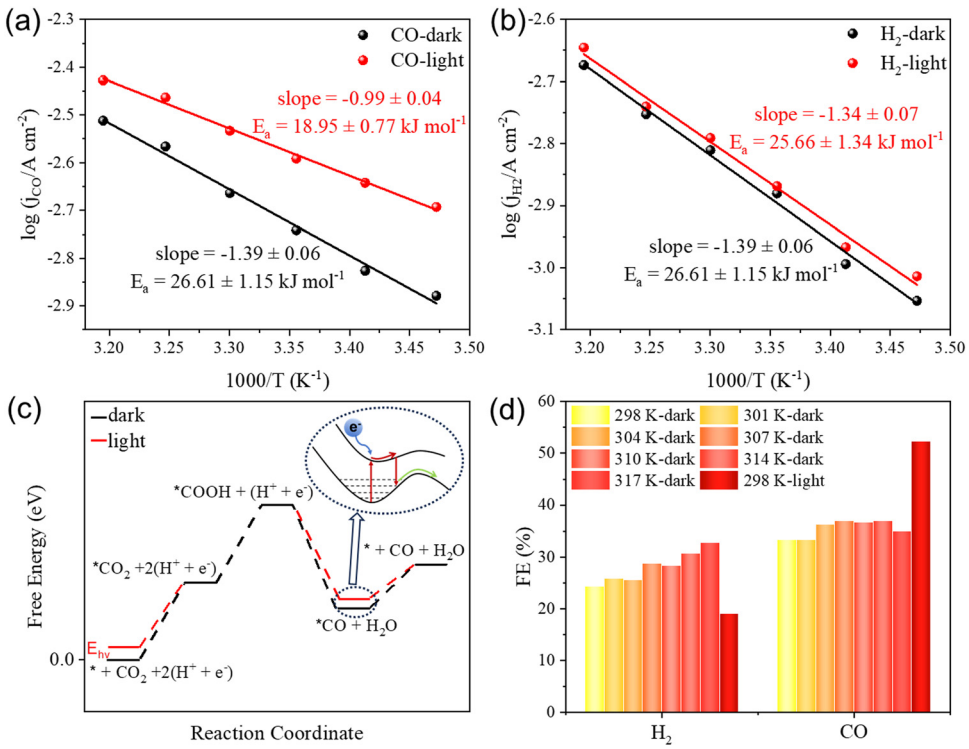

Fig. 5 Arrhenius plots of E_a for CO (a) and H_2 (b) under dark and light conditions. (c) Schematic of energetics of elementary reaction steps for the CO_2RR in the dark (black) and under light (red) conditions. (d) FE_{H2} and FE_{CO} at different temperatures under the dark conditions and under light at 298 K.

plasmon-generated E_{hv} exclusively reduced the E_a in the first step under light irradiation. Cu is widely acknowledged to possess moderate adsorption energy for CO, thereby facilitating the formation of multi-carbon products through C–C coupling. However, the FE of the C_2 product did not increase under light irradiation in this work (Fig. S17, ESI†), implying that the plasmon effect on Cu did not promote the coupling between *CO species. This phenomenon reminds us of the transient negative ion (TNI) theory in the study of plasmonic catalysis.[53,54] Specifically, the hot electrons generated by LSPR excitation can transfer to an unpopulated adsorbate state to form a TNI, and then the adsorbate shifts to the excited state. If the energy deposited in the adsorbate is insufficient to overcome the activation barrier, the electron will be released back to the metal and the adsorbate will return to the ground state with additional vibration energy. During this process, hot electrons do not participate in the reduction process and only provide additional energy to promote the desorption of the adsorbate. In the process of plasmon-assisted CO_2RR, the adsorbed CO was not further reduced by hot electrons to multi electron products, and an increase in the CO production rate was observed. Therefore, we hold that hot electrons only provide the energy to overcome the adsorption energy barrier of *CO through the TNI process.

Considering that light irradiation may cause an increase in the electrolyte temperature,[55] we investigated whether the alterations in temperature could cause changes in the FE of CO without light. The temperature-dependent variations of FE are shown in Fig. 5d. The FE of H_2 tended to increase with rising temperature, while the FE of CO remained unchanged across different temperatures. The results disclosed that an increase in temperature promoted faster kinetics of HER rather than CO_2RR.[56] Conversely, it was observed that light irradiation promoted the CO_2RR while suppressing the HER, which also ruled out the contribution of the photothermal effect to the CO_2RR.

3.5. Solar-driven PEC device for CO_2RR

The plasmonic Cu NAs exhibited broad light absorption characteristics, and we investigated the CO_2RR performance of the Cu NA photocathode at various wavelengths (475 nm, 550 nm, and 700 nm). Compared to the dark condition, the irradiation of all tested wavelengths led to an enhancement in photocurrents (Fig. S18, ESI†). Notably, excitation at different wavelengths also significantly improved the selectivity of CO (Fig. 6a). Inspired by this, we conducted a solar-driven PEC device that employed the Au/TiO_2 photoanode for OER and the Cu NA photocathode for CO_2RR (Fig. 6b). The cell was powered by a commercial Si solar cell with an output photovoltage of 2.5 V. The plasmonic Au/TiO_2 photoanode exhibited higher photocurrent stability than TiO_2 during the OER process due to

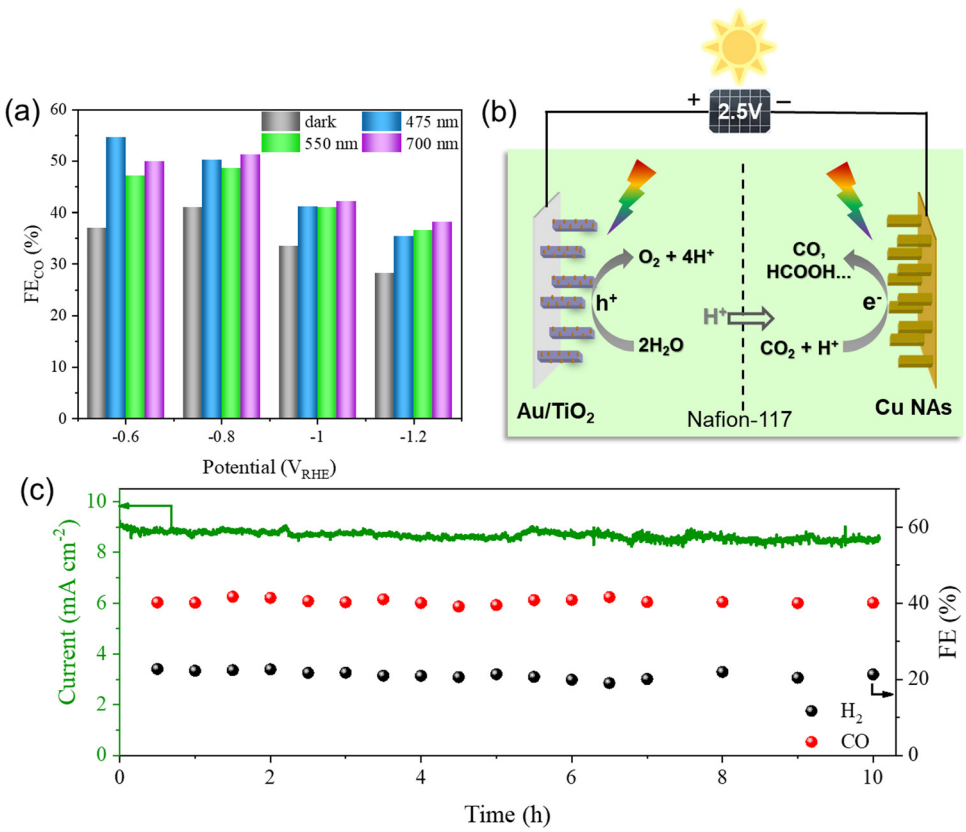

Fig. 6 (a) FE_{CO} of Cu NAs under different wavelengths with light intensity of 3.0 W cm^{-2} and under the dark conditions at different applied potentials. (b) Schematic diagram of solar-driven OER on the photoanode and CO_2RR on the photocathode. (c) Stability measurement of solar-driven PEC device for CO_2RR.

the generation of electron-rich surface states at the interfaces between Au and TiO_2, which was investigated in our previous work (Fig. S19, ESI†). We tested the stability of the Cu NA photocathode during the CO_2RR process. As shown in Fig. 6c, the FEs of CO (40%) and H_2 (20%), as well as the photocurrent density (8.8 mA cm^{-2}) remained stable during the 10 h of the test. Consequently, the syngas with a stable CO/H_2 molar ratio of 2 : 1 was obtained (Fig. S20, ESI†).

4. Conclusions

In summary, taking the Cu NA photocathode for the CO_2RR as a model system, the plasmonic effect on tuning CO_2 reduction activity and selectivity was investigated. Under plasmon excitation, the photocurrent density of the Cu NA photocathode was enhanced and the Tafel slope was reduced, which was attributed to the contribution of hot carriers. The accumulation of hot electrons resulted in the generation of E_{hv}, which selectively reduced the E_a of CO_2 to CO without affecting the HER. The designed solar-driven PEC device, composed of the plasmonic Cu NA photocathode and an Au/TiO_2 photoanode, exhibited good photostability and stable syngas composition (CO : H_2 = 2 : 1). These findings provide insight into the role of LSPR excitation in enhancing the electrocatalytic activity of nanostructured plasmonic metals and tuning the selectivity.

Author contributions

Y. Zhang directed the project. J. Xue carried out most of the experiments. Y. Zhang and J. Xue wrote the manuscript, with input from others. C. Zhen and K. Dang conducted the electron microscopy characterization and XRD experiments. L. Wu assisted in the EIS experiments. K. Dang assisted in the Raman experiments. All the authors analyzed the results and reviewed the paper.

Conflicts of interest

The authors declare no competing financial interest.

Acknowledgements

This work was supported by the National Key R&D Program of China (No. 2022YFA1505000), the National Natural Science Foundation of China (No. 22072158), the Strategic Priority Research Program of Chinese Academy of Sciences, Grant No. XDB36000000 and CAS Project for Young Scientists in Basic Research YSBR-004.

References

1 S. Linic, U. Aslam, C. Boerigter and M. Morabito, Photochemical Transformations on Plasmonic Metal Nanoparticles, *Nat. Mater.*, 2015, **14**, 567–576.
2 R. Nixon, E. Contreras and P. K. Jain, Electrochemistry with plasmons, *Trends Chem.*, 2023, **5**, 605–619.
3 P. Lyu, R. Espinoza and S. C. Nguyen, Photocatalysis of Metallic Nanoparticles: Interband *vs.* Intraband Induced Mechanisms, *J. Phys. Chem. C*, 2023, **127**, 15685–15698.
4 Z. Zhang, C. Zhang, H. Zheng and H. Xu, Plasmon-Driven Catalysis on Molecules and Nanomaterials, *Acc. Chem. Res.*, 2019, **52**, 2506–2515.
5 Y. Zhang, W. Guo, Y. Zhang and W. D. Wei, Plasmonic Photoelectrochemistry: In View of Hot Carriers, *Adv. Mater.*, 2021, **33**, 2006654–2006669.
6 Y. Zhang, S. He, W. Guo, Y. Hu, J. Huang, J. R. Mulcahy and W. D. Wei, Surface-Plasmon-Driven Hot Electron Photochemistry, *Chem. Rev.*, 2018, **118**, 2927–2954.
7 A. M. Brown, R. Sundararaman, P. Narang, W. A. Goddard and H. A. Atwater, Nonradiative Plasmon Decay and Hot Carrier Dynamics: Effects of Phonons, Surfaces, and Geometry, *ACS Nano*, 2015, **10**, 957–966.
8 Q. Hao, Z. Li, Y. Shi, R. Li, Y. Li, L. Wang, H. Yuan, S. Ouyang and T. Zhang, Plasmon-Induced Radical-Radical Heterocoupling Boosts Photodriven Oxidative Esterification of Benzyl Alcohol over Nitrogen-Doped Carbon-Encapsulated Cobalt Nanoparticles, *Angew. Chem., Int. Ed.*, 2023, **62**, e202312808.
9 A. J. Wilson, V. Mohan and P. K. Jain, Mechanistic Understanding of Plasmon-Enhanced Electrochemistry, *J. Phys. Chem. C*, 2019, **123**, 29360–29369.
10 X. Zhang, A. Fu, X. Chen, L. Liu, L. Ren, L. Tong and J. Ye, Highly Efficient Cu Induced Photocatalysis for Visible-light Hydrogen Evolution, *Catal. Today*, 2019, **335**, 166–172.
11 J. Xue, L. Wu, C. Deng, D. Tang, S. Wang, H. Ji, C. Chen, Y. Zhang and J. Zhao, Plasmon-Mediated Electrochemical Activation of Au/TiO_2 Nanostructure-Based Photoanodes for Enhancing Water Oxidation and Antibiotic Degradation, *ACS Appl. Nano Mater.*, 2022, **5**, 11342–11351.
12 Y. Zhang, Y. Zhang, W. Guo, A. C. Johnston-Peck, Y. Hu, X. Song and W. D. Wei, Modulating Multi-hole Reaction Pathways for Photoelectrochemical Water Oxidation on Gold Nanocatalysts, *Energy Environ. Sci.*, 2020, **13**, 1501–1508.
13 C. Zhan, Q.-X. Wang, J. Yi, L. Chen, D.-Y. Wu, Y. Wang, Z.-X. Xie, M. Moskovits and Z.-Q. Tian, Plasmonic Nanoreactors Regulating Selective Oxidation by Energetic Electrons and Nanoconfined Thermal Fields, *Sci. Adv.*, 2021, **7**, eabf0962.
14 A. Marimuthu, J. Zhang and S. Linic, Tuning Selectivity in Propylene Epoxidation by Plasmon Mediated Photo-Switching of Cu Oxidation State, *Science*, 2013, **339**, 1590–1593.
15 L. Zhou, D. F. Swearer, C. Zhang, H. Robatjazi, H. Zhao, L. Henderson, L. Dong, P. Christopher, E. A. Carter, P. Nordlander and N. J. Halas, Quantifying Hot Carrier and Thermal Contributions in Plasmonic Photocatalysis, *Science*, 2018, **362**, 69–72.
16 J. Wang, J. Heo, C. Chen, A. J. Wilson and P. K. Jain, Ammonia Oxidation Enhanced by Photopotential Generated by Plasmonic Excitation of a Bimetallic Electrocatalyst, *Angew. Chem., Int. Ed.*, 2020, **59**, 18430–18434.

17 F. Tong, X. Liang, Z. Wang, Y. Liu, P. Wang, H. Cheng, Y. Dai, Z. Zheng and B. Huang, Probing the Mechanism of Plasmon-Enhanced Ammonia Borane Methanolysis on a CuAg Alloy at a Single-Particle Level, *ACS Catal.*, 2021, **11**, 10814–10823.

18 F. Tong, X. Liang, M. Liu, Z. Wang, Y. Liu, P. Wang, H. Cheng, Y. Dai, Z. Zheng and B. Huang, Plasmon-Enhanced Water Activation for Hydrogen Evolution from Ammonia-Borane Studied at a Single-Particle Level, *ACS Catal.*, 2022, **12**, 3558–3565.

19 M. Lv, X. Zhang, B. Li, X. Gong, Y. Zhang, Z. Wang, Y. Liu, P. Wang, H. Cheng, Y. Dai, Y. Fan, B. Huang and Z. Zheng, Plasmonic Ag Interlayer Induced Direct Energy Transfer Studied at Single-Particle Level, *ACS Energy Lett.*, 2023, **8**, 4033–4042.

20 Y. Xin, K. Yu, L. Zhang, Y. Yang, H. Yuan, H. Li, L. Wang and J. Zeng, Copper-Based Plasmonic Catalysis: Recent Advances and Future Perspectives, *Adv. Mater.*, 2021, **33**, 2008145–2008170.

21 S. Jeong, Y. Liu, Y. Zhong, X. Zhan, Y. Li, Y. Wang, P. M. Cha, J. Chen and X. Ye, Heterometallic Seed-Mediated Growth of Monodisperse Colloidal Copper Nanorods with Widely Tunable Plasmonic Resonances, *Nano Lett.*, 2020, **20**, 7263–7271.

22 L. Li, Y. Zhang, T. Zhou, K. Wang, C. Wang, T. Wang, L. Yuan, K. An, C. Zhou and G. Lü, Mitigation of China's Carbon Neutrality to Global Warming, *Nat. Commun.*, 2022, **13**, 5315–5321.

23 Z. Liu, Z. Deng, G. He, H. Wang, X. Zhang, J. Lin, Y. Qi and X. Liang, Challenges and Opportunities for Carbon Neutrality in China, *Nat. Rev. Earth Environ.*, 2021, **3**, 141–155.

24 T. Le, Y. Shao and B. Wang, Plasmon-Induced CO_2 Conversion on Al@Cu_2O: A DFT Study, *J. Phys. Chem. C*, 2021, **125**, 6108–6115.

25 Z. Wang, H. Song, H. Pang, Y. Ning, T. D. Dao, Z. Wang, H. Chen, Y. Weng, Q. Fu, T. Nagao, Y. Fang and J. Ye, Photo-Assisted Methanol Synthesis via CO_2 Reduction under Ambient Pressure over Plasmonic Cu/ZnO Catalysts, *Appl. Catal., B*, 2019, **250**, 10–16.

26 M. P. S. Rodrigues, A. H. B. Dourado, A. G. Sampaio de Oliveira-Filho, A. P. de Lima Batista, M. Feil, K. Krischer and S. I. Córdoba de Torresi, Gold–Rhodium Nanoflowers for the Plasmon-Enhanced CO_2 Electroreduction Reaction upon Visible Light, *ACS Catal.*, 2022, **13**, 267–279.

27 Y. Kim, E. B. Creel, E. R. Corson, B. D. McCloskey, J. J. Urban and R. Kostecki, Surface-Plasmon-Assisted Photoelectrochemical Reduction of CO_2 and NO_3^- on Nanostructured Silver Electrodes, *Adv. Energy Mater.*, 2018, **8**, 1800363.

28 E. B. Creel, E. R. Corson, J. Eichhorn, R. Kostecki, J. J. Urban and B. D. McCloskey, Directing Selectivity of Electrochemical Carbon Dioxide Reduction Using Plasmonics, *ACS Energy Lett.*, 2019, **4**, 1098–1105.

29 W. Ou, B. Zhou, J. Shen, T. W. Lo, D. Lei, S. Li, J. Zhong, Y. Y. Li and J. Lu, Thermal and Nonthermal Effects in Plasmon-Mediated Electrochemistry at Nanostructured Ag Electrodes, *Angew. Chem., Int. Ed.*, 2020, **59**, 6790–6793.

30 X. Zhang, X. Li, M. E. Reish, D. Zhang, N. Q. Su, Y. Gutiérrez, F. Moreno, W. Yang, H. O. Everitt and J. Liu, Plasmon-Enhanced Catalysis: Distinguishing Thermal and Nonthermal Effects, *Nano Lett.*, 2018, **18**, 1714–1723.

31 W. Ou, Y. Fan, J. Shen, Y. Xu, D. Huang, B. Zhou, T. W. Lo, S. Li, Y. Y. Li, D. Lei and J. Lu, Plasmoelectric Potential in Plasmon-Mediated Electrochemistry, *Nano Lett.*, 2022, **22**, 8397–8405.

32 C. Zhan, B.-W. Liu, Y.-F. Huang, S. Hu, B. Ren, M. Moskovits and Z.-Q. Tian, Disentangling Charge Carrier from Photothermal Effects in Plasmonic Metal Nanostructures, *Nat. Commun.*, 2019, **10**, 2671–2678.

33 E. Cortés, R. Grzeschik, S. A. Maier and S. Schlücker, Experimental Characterization Techniques for Plasmon-Assisted Chemistry, *Nat. Rev. Chem.*, 2022, **6**, 259–274.

34 K. P. Kuhl, E. R. Cave, D. N. Abram and T. F. Jaramillo, New Insights into the Electrochemical Reduction of Carbon Dioxide on Metallic Copper Surfaces, *Energy Environ. Sci.*, 2012, **5**, 7050–7059.

35 H. Xiong, Q. Sun, K. Chen, Y. Xu, X. Chang, Q. Lu and B. Xu, Correlating the Experimentally Determined CO Adsorption Enthalpy with the Electrochemical CO Reduction Performance on Cu Surfaces, *Angew. Chem., Int. Ed.*, 2023, **62**, e202218447.

36 Y. Yang, S. Louisia, S. Yu, J. Jin, I. Roh, C. Chen, M. V. Fonseca Guzman, J. Feijóo, P.-C. Chen, H. Wang, C. J. Pollock, X. Huang, Y.-T. Shao, C. Wang, D. A. Muller, H. D. Abruña and P. Yang, Operando Studies Reveal Active Cu Nanograins for CO_2 Electroreduction, *Nature*, 2023, **614**, 262–269.

37 J. L. Duan, T. W. Cornelius, J. Liu, S. Karim, H. J. Yao, O. Picht, M. Rauber, S. Müller and R. Neumann, Surface Plasmon Resonances of Cu Nanowire Arrays, *J. Phys. Chem. C*, 2009, **113**, 13583–13587.

38 Y. Zhou, Y. Liang, J. Fu, K. Liu, Q. Chen, X. Wang, H. Li, L. Zhu, J. Hu, H. Pan, M. Miyauchi, L. Jiang, E. Cortés and M. Liu, Vertical Cu Nanoneedle Arrays Enhance the Local Electric Field Promoting C_2 Hydrocarbons in the CO_2 Electroreduction, *Nano Lett.*, 2022, **22**, 1963–1970.

39 C. Choi, S. Kwon, T. Cheng, M. Xu, P. Tieu, C. Lee, J. Cai, H. M. Lee, X. Pan, X. Duan, W. A. Goddard III and Y. Huang, Highly Active and Stable Stepped Cu Surface for Enhanced Electrochemical CO_2 Reduction to C_2H_4, *Nat. Catal.*, 2020, **3**, 804–812.

40 J. Feijóo, Y. Yang, M. V. Fonseca Guzman, A. Vargas, C. Chen, C. J. Pollock and P. Yang, Operando High-Energy-Resolution X-ray Spectroscopy of Evolving Cu Nanoparticle Electrocatalysts for CO_2 Reduction, *J. Am. Chem. Soc.*, 2023, **145**, 20208–20213.

41 O. van der Heijden, S. Park, J. J. J. Eggebeen and M. T. M. Koper, Non-Kinetic Effects Convolute Activity and Tafel Analysis for the Alkaline Oxygen Evolution Reaction on NiFeOOH Electrocatalysts, *Angew. Chem., Int. Ed.*, 2023, **62**, e202216477.

42 S. Yu and P. K. Jain, The Chemical Potential of Plasmonic Excitations, *Angew. Chem., Int. Ed.*, 2019, **59**, 2085–2088.

43 C. Xu, X. Zhang, M.-N. Zhu, L. Zhang, P.-F. Sui, R. Feng, Y. Zhang and J.-L. Luo, Accelerating Photoelectric CO_2

Conversion with a Photothermal Wavelength-Dependent Plasmonic Local Field, *Appl. Catal., B*, 2021, **298**, 120533.

44 Z. Lyu, S. Zhu, M. Xie, Y. Zhang, Z. Chen, R. Chen, M. Tian, M. Chi, M. Shao and Y. Xia, Controlling the Surface Oxidation of Cu Nanowires Improves Their Catalytic Selectivity and Stability toward C^{2+} Products in CO_2 Reduction, *Angew. Chem., Int. Ed.*, 2021, **60**, 1909–1915.

45 Y. Zhao, X.-G. Zhang, N. Bodappa, W.-M. Yang, Q. Liang, P. M. Radjenovica, Y.-H. Wang, Y.-J. Zhang, J.-C. Dong, Z.-Q. Tian and J.-F. Li, Elucidating Electrochemical CO_2 Reduction Reaction Processes on Cu(*hkl*) Single-Crystal Surfaces by in situ Raman Spectroscopy, *Energy Environ. Sci.*, 2022, **15**, 3968–3977.

46 I. V. Chernyshova, P. Somasundaran and S. Ponnurangam, On the Origin of the Elusive First Intermediate of CO_2 Electroreduction, *Proc. Natl. Acad. Sci. U. S. A.*, 2018, **115**, E9261–E9270.

47 Z. Lyu, S. Zhu, M. Xie, Y. Zhang, Z. Chen, R. Chen, M. Tian, M. Chi, M. Shao and Y. Xia, Controlling the Surface Oxidation of Cu Nanowires Improves Their Catalytic Selectivity and Stability toward C^{2+} Products in CO_2 Reduction, *Angew. Chem., Int. Ed.*, 2021, **60**, 1909–1915.

48 B. Chang, Z. Min, N. Liu, N. Wang, M. Fan, J. Fan and J. Wang, Electrocatalytic CO_2 Reduction to Syngas, *Green Energy Environ.*, 2023, DOI: **10.1016/j.gee.2023.05.005**.

49 Y. Xu, W. Liu, Z. Xu, Y. Zhou and X.-Y. Yu, In situ Reconstructed $AgZn_3$ Nanoparticles Supported on Zinc Nanoplates for Efficient CO_2 Electroreduction to Tunable Syngas, *Chem. Commun.*, 2023, **59**, 8596–8599.

50 B. Zhao, X. Huang, Y. Ding and Y. Bi, Bias-Free Solar-Driven Syngas Production: A Fe_2O_3 Photoanode Featuring Single-Atom Cobalt Integrated with a Silver-Palladium Cathode, *Angew. Chem., Int. Ed.*, 2022, **62**, e202213067.

51 Y. Kim, D. Dumett Torres and P. K. Jain, Activation Energies of Plasmonic Catalysts, *Nano Lett.*, 2016, **16**, 3399–3407.

52 Y. Jia, H.-S. Hsu, W.-C. Huang, D.-W. Lee, S.-W. Lee, T.-Y. Chen, L. Zhou, J.-H. Wang, K.-W. Wang and S. Dai, Probing the Roles of Indium Oxides on Copper Catalysts for Enhanced Selectivity during CO_2-to-CO Electrochemical Reduction, *Nano Lett.*, 2023, **23**, 2262–2268.

53 S. Linic, P. Christopher and D. B. Ingram, Plasmonic-Metal Nanostructures for Efficient Conversion of Solar to Chemical Energy, *Nat. Mater.*, 2011, **10**, 911–921.

54 U. Aslam, V. G. Rao, S. Chavez and S. Linic, Catalytic Conversion of Solar to Chemical Energy on Plasmonic Metal Nanostructures, *Nat. Catal.*, 2018, **1**, 656–665.

55 R. E. Vos, K. E. Kolmeijer, T. S. Jacobs, W. van der Stam, B. M. Weckhuysen and M. T. M. Koper, How Temperature Affects the Selectivity of the Electrochemical CO_2 Reduction on Copper, *ACS Catal.*, 2023, **13**, 8080–8091.

56 S. T. Ahn, I. Abu-Baker and G. T. R. Palmore, Electroreduction of CO_2 on Polycrystalline Copper: Effect of Temperature on Product Selectivity, *Catal. Today*, 2017, **288**, 24–29.